JPhys Photonics

PAPER • OPEN ACCESS

Mid-infrared fused fiber optics: a fluoride coupler for 5000 nm applications

To cite this article: Francesco Anelli *et al* 2025 *J. Phys. Photonics* **7** 045010

Journal of Physics: Photonics

OPEN ACCESS

RECEIVED
3 July 2025

REVISED
25 July 2025

ACCEPTED FOR PUBLICATION
26 August 2025

PUBLISHED
5 September 2025

PAPER

Mid-infrared fused fiber optics: a fluoride coupler for 5000 nm applications

Francesco Anelli[1], **Andrea Annunziato**[1], **Jean Letourneur**[2], **Solenn Cozic**[2] and **Francesco Prudenzano**[1,*]

[1] Department of Electrical and Information Engineering, Politecnico di Bari, Bari, Italy
[2] Le Verre Fluoré, Bruz, France
[*] Author to whom any correspondence should be addressed.

E-mail: francesco.prudenzano@poliba.it

Keywords: optical fiber coupler, fused biconical taper, fluoride fiber, mid-infrared, soft glass

Abstract

A 2 × 2 optical fiber coupler is manufactured by employing two single-mode indium fluoride optical fibers enclosed within a low-refractive-index indium fluoride capillary. The design leverages the finite element method to calculate the phase constants of the x and y polarized components of the symmetric and antisymmetric supermodes guided through the whole waveguiding region. The fabricated polarization independent coupler is characterized in the mid-infrared wavelength range up to 5000 nm, demonstrating about 3 dB coupling at this record-high wavelength. The numerical investigations show how both the degree of glass fusion and the capillary affect the coupling length and the coupler sensitivity to the polarization. In particular, for the first time, the influence of the capillary is investigated and discussed improving the understanding of the coupling phenomenon. These results pave the way for obtaining optical devices with enhanced performance in applications such as spectroscopy, medical diagnostics and therapy.

1. Introduction

Optical fiber couplers play a critical role in a wide range of applications serving as a wavelength division multiplexer/demultiplexer, polarization beam splitter, sensor, etc [1–5]. The commercialized silica optical fiber couplers are limited by the glass intrinsic absorption, making them unsuitable for applications at wavelengths exceeding $\lambda \simeq 2.0\,\mu$m [6, 7]. The demand for robust and efficient mid-infrared optical fiber couplers is driven by the unique advantages of these wavelengths, including strong molecular absorption fingerprints, medical diagnostics, and thermal imaging [8–11]. One of the most employed coupler fabrication techniques involves laterally fusing and simultaneously stretching a pair of uncoated fibers over a short length using a high-temperature heater [1, 12]. The same technique can be applied to soft glasses operating in the mid-infrared, e.g. fluoride and chalcogenide [13]. In particular, developing optical fiber components with fluoride glass is strongly desirable because of the lower refractive index, larger optical damage threshold and lower non-linear refractive index than chalcogenide glass [14–16]. Despite recent advancements in both fluoride [17–19], and chalcogenide glasses [20–22], the development of couplers capable of operating within the mid-infrared spectral range continues to pose significant challenges. Several issues remain to be addressed to develop market-ready fluoride couplers, including: (i) the mechanical fragility of the coupler, which limits its handling [23]; (ii) the challenge of achieving precise control over the coupling ratio to meet application requirements. Recently, the use of a low-refractive-index capillary in combination with two multimode optical fibers has been proposed [17]. This is considered a potential solution to the issue (i) [23]. However, it is crucial to analyze how the introduction of the capillary affects the electromagnetic modes involved in the coupling process. This can be achieved by examining the impact of unconventional waist geometry, consisting of both the optical fibers and the surrounding capillary. An accurate electromagnetic investigation is required to enhance the understanding of the coupling mechanism and, ultimately, achieve more precise control over the coupling ratio.

In this paper, a mid-infrared compatible 2×2 optical fiber coupler is designed using finite element method (FEM) and supermode theory, focusing on the impact of fusion degree and capillary thickness on the performance. The device is fabricated using the stretching and heating technique, inserting single-mode indium fluoride optical fibers in a custom indium fluoride capillary, which has a refractive index lower than the cladding refractive index. The employed materials are manufactured by Le Verre Fluoré, Bruz, France. To the best of our knowledge, this is the first single-mode fluoride optical fiber coupler to be characterized over a broadband spectrum up to 5000 nm. The fabricated device can boost a wide range of applications, including mid-infrared sensing, fiber lasers, and medical diagnostics/treatment.

2. Theory of the optical fiber coupling

The most used analytical approach to design a coupler is based on the coupled mode theory, assuming that the two optical fibers are parallel and interact weakly, via evanescent coupling [24, 25]. Therefore, the modal solution of the unperturbed waveguide is employed, then considering the influence of the perturbation due to the presence of another waveguide [26]. Nevertheless, this method is increasingly inaccurate as the waveguides get closer and smaller, i.e. for strong coupling, and makes it more complicated to analyze the eventual coupler sensitivity to the state of polarization of the light [2]. In our analysis, the supermodes are calculated considering the whole cross-section in the coupling section, i.e. waist region, of the coupler [27].

When the adiabatic criterion is satisfied, no higher order modes are excited in the tapered transitions [28, 29]. Based on this hypothesis, the power coupling occurs due to the beating between the symmetric (or even) and antisymmetric (or odd) supermodes in the waist region of the composite waveguide, formed by the two optical fibers [30]. The coupling coefficient C for the polarization x/y of the symmetric $(+)$ and antisymmetric supermode $(-)$ is defined as the half difference between their propagation constants β [30, 31]:

$$C_{x/y}(z,\lambda) = \frac{\beta^{+}_{x/y}(z,\lambda) - \beta^{-}_{x/y}(z,\lambda)}{2}. \tag{1}$$

The powers at the cross port $P_{\mathrm{C}x/y}(\lambda)$ and at the through port $P_{\mathrm{T}x/y}(\lambda)$ at the output of the device can be easily calculated for each polarization as [2]:

$$P_{\mathrm{C}x/y}(\lambda) = \sin^2 \int_0^L C_{x/y}(z,\lambda)\,\mathrm{d}z \tag{2}$$

$$P_{\mathrm{T}x/y}(\lambda) = \cos^2 \int_0^L C_{x/y}(z,\lambda)\,\mathrm{d}z. \tag{3}$$

For a particular geometry, constant along the longitudinal direction z, the coupling length $L_{\mathrm{c}}(\lambda)$, which represents the distance over which full power transfer occurs between the two fibers, is dependent on the coupling coefficient [31]:

$$L_{\mathrm{c}x/y}(\lambda) = \frac{\pi}{\beta^{+}_{x/y}(\lambda) - \beta^{-}_{x/y}(\lambda)} = \frac{\pi}{2 \times C_{x/y}(\lambda)}. \tag{4}$$

The coupling takes place along the waist region of the taper, having length L_{w}. In this analysis, the degree of fusion f is a critical factor that must be considered to accurately account for the complex geometry of the fused region [1].

The degree of fusion f can be defined as [27]:

$$f = \frac{2 \times r_{\mathrm{cl}} - d_{\mathrm{c-c}}}{2 \times \left(2 - \sqrt{2}\right) \times r_{\mathrm{cl}}} \tag{5}$$

where r_{cl} is the tapered cladding radius of each fiber and $d_{\mathrm{c-c}}$ is the center-to-center distance of the two optical fibers, in the waist region. In other words, $f = 0$ (i.e. $2 \times r_{\mathrm{cl}} = d_{\mathrm{c-c}}$) implies tangent fibers, which is the weakest fusion, and $f = 1$ determines a single circular cross section with two cores, which is the case characterized by the strongest fusion. In this model, a coupler can assume any cross-sectional shape between these two extremes, depending on the fabrication parameters used [1]. Based on material conservation, the overlapped area is exactly redistributed to the surrounding region by incorporating circular arcs [27], as illustrated in figure 1 for different degrees of fusion f. In this method, the geometry of the device can be easily considered using mode solving software based on FEM, finite difference time domain method, beam propagation method, etc.

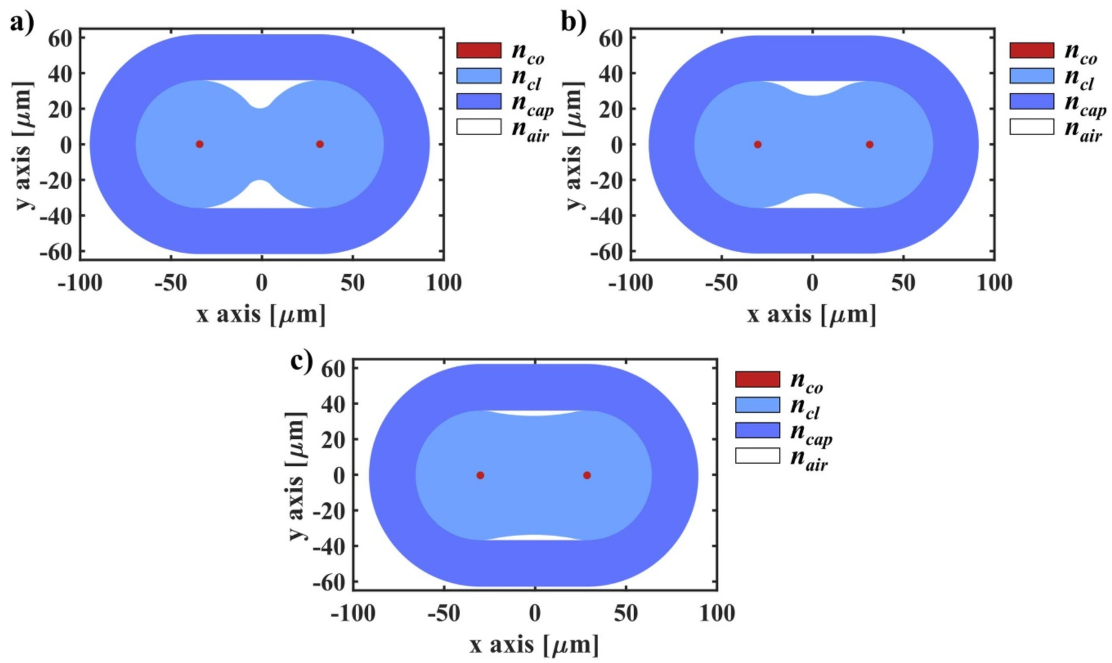

Figure 1. Refractive index distribution of the 2×2 single-mode optical fiber coupler for different degrees of fusion f, (a) $f = 0.1$, (b) $f = 0.2$, (c) $f = 0.3$.

3. Design of the 2×2 indium fluoride optical fiber coupler

In this Section, a symmetrical 2×2 single-mode optical fiber coupler with indium fluoride (InF_3) glass is modeled. The device can be fabricated by employing a hosting low refractive index capillary. The design aims at achieving a 3-dB coupler operating at the wavelength $\lambda = 5000$ nm. The commercial optical fibers are the IFG 7.5/125 from Le Verre Fluoré, with core diameter $d_{co} = 7.5\,\mu$m, and cladding diameter $d_{cl} = 125\,\mu$m. The numerical aperture is NA $= 0.3$, which guarantees single-mode operation from the wavelength $\lambda \simeq 2.95\,\mu$m. Full vector FEM is employed to study also the eventual polarization dependence. The material dispersion of the capillary, cladding and core refractive index as a function of the wavelength λ is taken into account [32]. The maximum triangular mesh element size $T_{ms} = 0.5\,\mu$m is well below the operating wavelength λ. The tapering ratio TR, defined as the ratio of untapered to tapered diameters, is selected. To this aim, a single tapered optical fiber is considered under the assumption that both the core-to-cladding ratio and the refractive indices of the core and cladding remain unchanged. In particular, the tapering ratio TR $= 1.8$ is chosen, ensuring that the effective refractive index n_{eff} of the LP_{01} mode at the wavelength $\lambda = 5\,\mu$m is close to the cladding refractive index n_{cl} at the same wavelength. This determines a low confinement of the mode and the possibility to couple to the other optical fiber.

The maximum taper angle $\Omega(z)$ has been evaluated taking into account in the calculation the phase constant of the LP_{01} and LP_{11} modes [33]. In particular, considering the wavelength $\lambda = 5\,\mu$m and the tapering ratio $TR = 1.8$, the calculated maximum taper angle is $\Omega = 0.12°$, implying tapered transitions longer than $L_T = 1.8$ cm.

Then, considering the tapering ratio TR $= 1.8$, the waist of the symmetrical 2×2 single-mode optical fiber coupler based on indium fluoride glass is modeled, as sketched in figure 1.

In the 2D simulation, the capillary with a thickness $t_{cap} = 25\,\mu$m encloses two internal optical fibers characterized by different degrees of fusion from $f = 0.1$ to $f = 0.3$, with a sampling step $\Delta f = 0.05$. As outlined in section 2, the degree of fusion f quantitatively describes the extent of thermal merging between the optical fibers. In this study, only low fusion levels are considered to represent partially merged configurations where the individual fiber geometries are still largely distinguishable. This choice is motivated by practical considerations related to fluoride glass. Achieving high levels of fusion typically requires elevated temperatures; however, fluoride glass is highly sensitive to thermal processing and tends to gradually devitrify when heated to temperature between the glass transition temperature and the melting temperature [34–36]. Therefore, low-fusion regimes are both physically realistic and more suitable for preserving the integrity of fluoride glass during fabrication. For simplicity, the capillary is modeled with two circular and

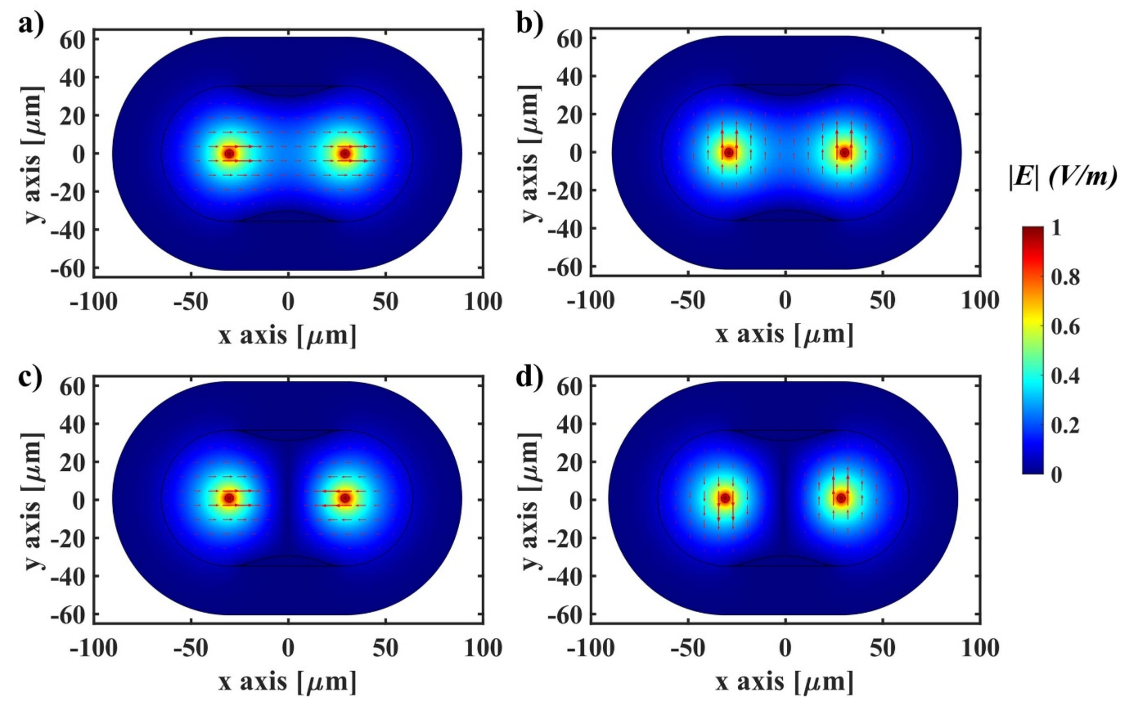

Figure 2. Simulated electric field norm $|E|\ (\mathrm{V\,m^{-1}})$ of the x and y polarized components of the symmetric and antisymmetric supermodes calculated at the wavelength $\lambda = 5000$ nm for degree of fusion $f = 0.25$, (a) x polarized component of the symmetric supermode, (b) y polarized component of the symmetric supermode, (c) x polarized component of the antisymmetric supermode, (d) y polarized component of the antisymmetric supermode; the red arrows represent the x and y components of the electric field E.

two straight sections. The simulation is performed from the wavelength $\lambda = 2700$ nm to $\lambda = 5000$ nm with a sampling step $\Delta\lambda = 50$ nm, considering the dispersion versus the wavelength λ of the refractive indices.

Figure 2 reports the electric field norm $|E|\ (V/m)$ of the x and y polarizations of both symmetric and antisymmetric supermodes calculated at the wavelength $\lambda = 5000$ nm for degree of fusion $f = 0.25$. The simulation also includes a surrounding air domain with a perfectly matched layer. At $\lambda = 5000$ nm, the effective refractive index for the x polarized component of the symmetric supermode (figure 2(a)) is $n_{\mathrm{eff}} \simeq 1.448428$, for the y polarized component of the symmetric supermode (figure 2(b)) is $n_{\mathrm{eff}} \simeq 1.448424$, for the x polarized component of the antisymmetric supermode (figure 2(c)) is $n_{\mathrm{eff}} \simeq 1.448296$, and for the y polarized component of the antisymmetric supermode (figure 2(d)) is $n_{\mathrm{eff}} \simeq 1.448294$.

Figure 3 reports the simulated coupling length L_c of the x polarized components (solid line) and of the y polarized components (dashed line) as a function of the wavelength λ for different degrees of fusion f. Only coupling lengths $L_c < 10$ cm are reported, which are more desirable for compactness and for reducing the fabrication complexity. As expected, the coupling length L_c decreases as the degree of fusion f increases [27]. Moreover, the chosen tapering ratio TR allows an operation that is practically polarization independent.

The influence of the capillary on the coupling phenomenon is investigated for the first time. Figure 4 shows the coupling length L_c of the x polarized components (solid line) and of the y polarized components (dashed line) as a function of the wavelength λ for 2×2 single-mode optical fiber coupler with degree of fusion $f = 0.25$ with and without capillary. The absence of the capillary causes power transfer to occur sooner. The thickness of the capillary, if larger than a few micrometers, has a negligible influence on the coupling length L_c. Indeed, by simulations, the coupling length L_c for $t_{\mathrm{cap}} = 10\,\mu$m is practically overlapped with those for $t_{\mathrm{cap}} = 25\,\mu$m and $t_{\mathrm{cap}} = 50\,\mu$m.

With the considered tapering ratio TR and degree of fusion f, the coupler does not exhibit sensitivity to the polarization of the modes both with and without the capillary.

Figure 5 shows the power of the through and cross output ports as a function of the waist length L_w when the input port is excited with x or y polarized light for degree of fusion $f = 0.25$, capillary thickness $t_{\mathrm{cap}} = 25\,\mu$m, and wavelength $\lambda = 5000$ nm. 3 dB coupling can be obtained for waist length $L_w \simeq 11.5$ mm.

The spectral behavior of the coupler with this waist length value L_w is reported in figure 6, demonstrating that no coupling occurs up to approximately $\lambda = 4\,\mu$m and then, the power of the excited input fiber is increasingly coupled to the other fiber.

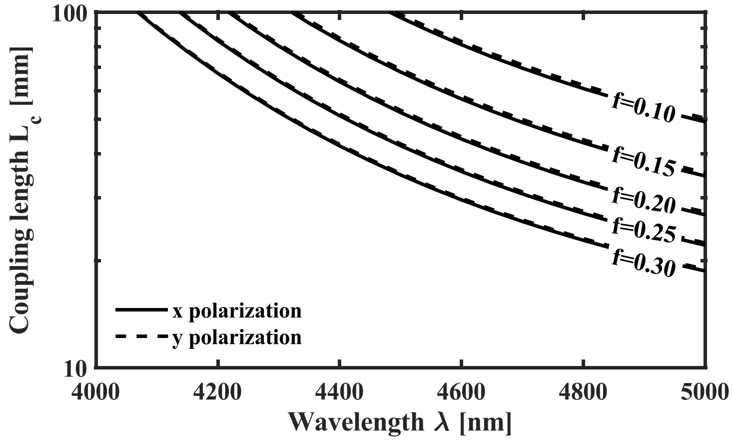

Figure 3. Simulated coupling length L_c of the x polarized components (solid line) and of the y polarized components (dashed line) as a function of the wavelength λ for different degrees of fusion f.

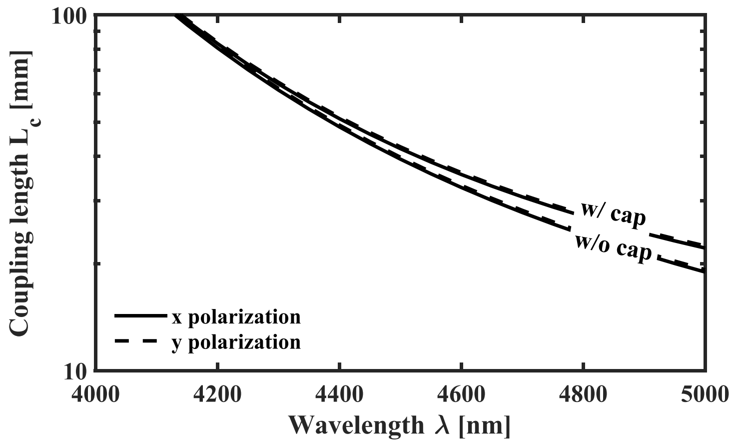

Figure 4. Simulated coupling length L_c of the x polarized components (solid line) and of the y polarized components (dashed line) as a function of the wavelength λ for 2×2 single-mode optical fiber coupler with degree of fusion $f = 0.25$, with and without capillary.

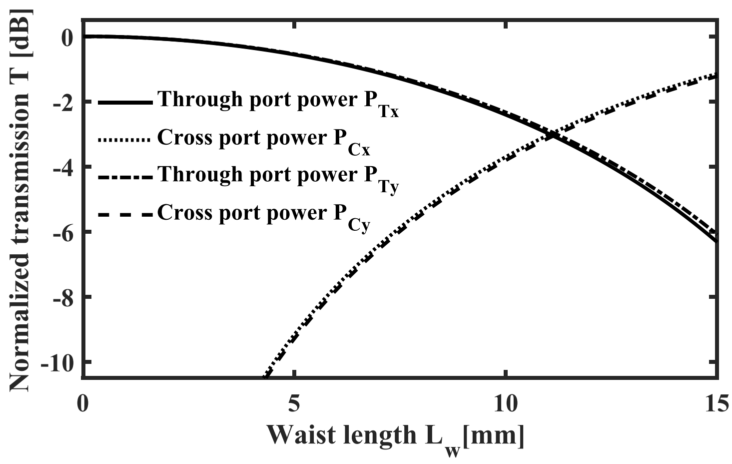

Figure 5. Simulated normalized transmission T of the through and cross output ports as a function of the waist length L_w when the input port is excited with x or y polarized light for degree of fusion $f = 0.25$ at the wavelength $\lambda = 5000$ nm.

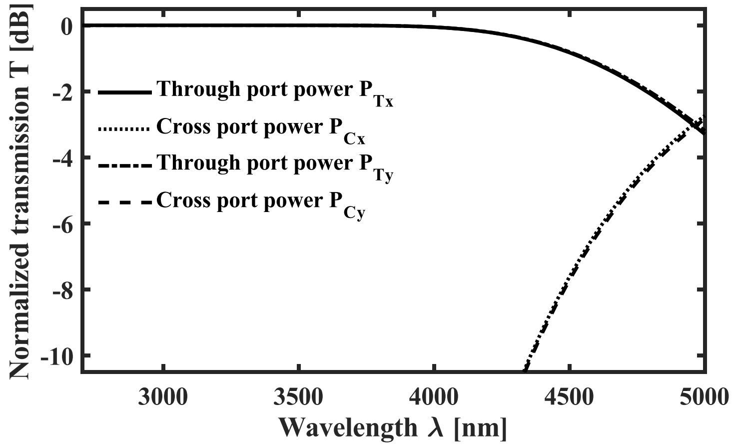

Figure 6. Simulated normalized transmission T of the through and cross output ports as a function of the wavelength λ when the input port is excited with x or y polarized light for degree of fusion $f = 0.25$ and waist length $L_w = 11.5$ mm.

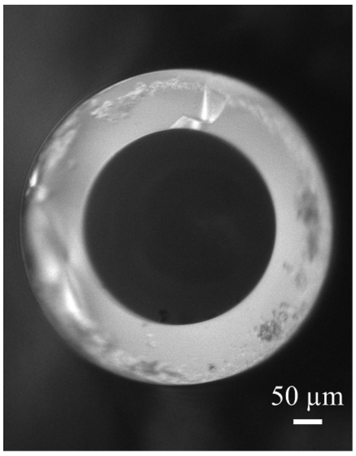

Figure 7. Cross-section of the indium fluoride low-refractive index capillary.

Although the current design is optimized for operation around $\lambda = 5\,\mu$m, increasing the tapering ratio TR and/or extending the waist length L_w could enable efficient coupling at shorter wavelengths.

4. Fabrication and characterization of the 2 × 2 indium fluoride optical fiber coupler

Apart from the use of low heating temperature to be very finely controlled for a successful fabrication and the adoption of the capillary, the manufacturing process is similar to that employed for silica glass based optical fiber couplers [37]. It can be summarized in the following steps: (i) two segments of IFG 7.5/125 optical fibers with length $L \simeq 80$ cm are stripped, cleaved and cleaned with isopropanol; (ii) the segments are inserted in the low-refractive index capillary, whose cross-section is reported in figure 7; (iii) the obtained structure is mounted on the fiber holding blocks of the glass processing system; (iv) the structure is pretensioned up to about $T = 15$ g by shifting one fiber holding block by a few micrometers while leaving the other fixed; (v) controlled stretching at a pulling speed $v = 500\,\mu\mathrm{m\,s^{-1}}$ combined with heating near the glass transition temperature $T_g \simeq 275\,^\circ$C, achieved by powering the graphite filament at approximately $P_{\mathrm{fil}} = 12$ W and by maintaining an argon flow rate $F_{\mathrm{Ar}} = 0.35\,\mathrm{l\,min^{-1}}$, allow the formation of the fused biconical taper. During the drawing, an interband cascade laser operating at the wavelength $\lambda = 3.34\,\mu$m is injected into one of the input ports, in order to measure the losses induced during the fabrication process. The overall power at the output ports is monitored during the process via Thorlabs PM100D console equipped with Thorlabs S401C thermal power sensor, achieving an excess loss EL < 0.6 dB at this wavelength.

Figure 8 presents a montage of micropictures giving the longitudinal view of the fused biconical taper. The images highlight carefully controlled gradual transitions in the down-taper and up-taper regions, as well as the uniform geometry of the waist.

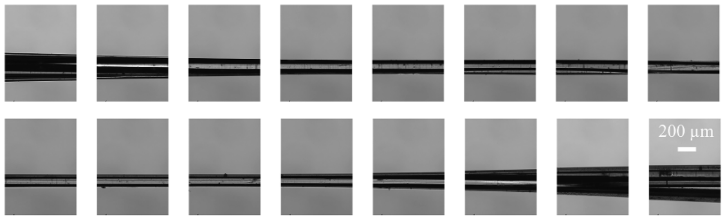

Figure 8. Montage of longitudinal pictures of the fabricated 2 × 2 single-mode optical fiber coupler, reported with a sampling step of 1600 μm.

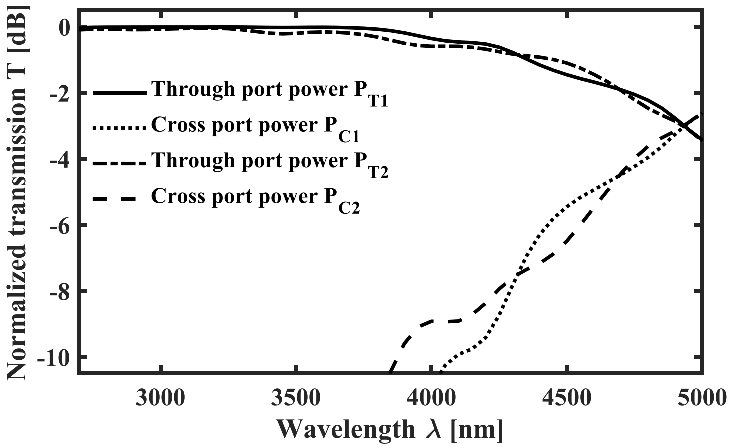

Figure 9. Measured normalized transmission T of the through and cross ports as a function of the wavelength λ when the input port is excited with unpolarized light.

For the coupling ratio characterization, a setup based on broadband halogen lamp, monochromator, high-sensitivity InSb power meter, and lock-in amplifier is employed. The light exiting the monochromator is coupled into a single-mode indium fluoride injection fiber using lenses. The coated injection fiber is sufficiently long to suppress any cladding modes that may be excited. The other end of the injection fiber is then aligned with one of the input fibers of the optical fiber coupler by means of a triaxial stage, ensuring coupling losses below 1 dB. Four measurements are conducted, assessing the power from the two output ports (i.e. through and cross) when each input optical fiber is excited individually.

Figure 9 reports the measured output powers for the through and cross ports, confirming good agreement with the numerical design. The measurements demonstrate broadband behavior and a 3 dB coupling at the wavelength $\lambda \simeq 4950$ nm. Considering the typical 50 : 50 coupling ratio tolerance of $\pm$ 6.0 % (i.e. coupling ratios from 56 : 44 to 44 : 56), the measured bandwidth of the fabricated coupler is about BW = 200 nm, proving its wideband operation. The slight difference in cross-port power, observed between the two separate measurements when each input fiber is excited, can be mainly attributed to low signal level causing increased detector noise.

The optical fiber coupler is then manually cleaved in the waist region to examine the geometry of the coupling section. The micropicture is shown in figure 10, where two closely positioned optical fibers are visible, with a degree of fusion close to $f = 0.25$, inferred by evaluating its geometrical features. It is not meaningful to focus on the flaws on the right fiber and on the scribe marks on the capillary which are related to the manual cleaving. Instead, it is important to assess the equal geometrical shape of the two fibers. This symmetry is further supported by the observation that the coupling is similar for both input ports.

Table 1 reports the comparison of the proposed device with other optical fiber couplers based on fluoride glass, including both zirconium fluoride (ZBLAN) and indium fluoride (InF_3) materials. In particular, this paper is the only one providing a broadband measurement in the upper transparency limits of the glass. This is because, even though in [19]. the tungsten lamp Thorlabs SLS202L with wavelength spanning from $\lambda = 450$ nm to $\lambda = 5500$ nm is employed, the spectrum was not recorded. Instead, just the overall power was measured with a Thorlabs S145C integrating sphere photodiode, which is sensitive only in the wavelength range from $\lambda = 800$ nm to $\lambda = 1700$ nm. An advantage of the proposed coupler is its enhanced mechanical robustness, made possible by the exploitation of the capillary.

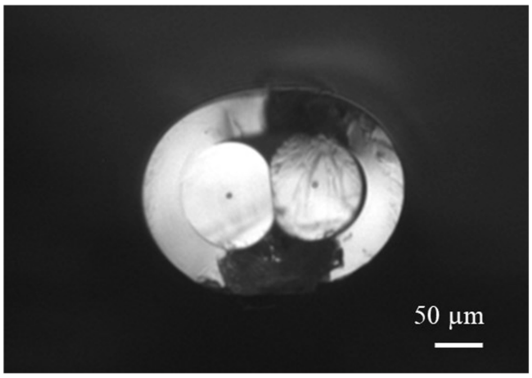

Figure 10. Cross-section of the 2 × 2 single-mode optical fiber coupler in the waist region.

Table 1. Comparison with fluoride optical fiber couplers.

References	Material	Light propagation	Tested wavelength	Coupling ratio (wavelength)
[13]	ZBLAN	Multi-mode	2000 nm	50 : 50 (2000 nm)
[19]	InF_3	Multi-mode	[450, 5500] nm	45 : 55 (1700 nm)
[17]	InF_3	Few-mode	3340 nm	73 : 27 (3340 nm)
[38]	InF_3	Single-mode	3340 nm	48 : 52 (3340 nm)
[18]	ZBLAN	Single-mode	[1500, 3000] nm	41 : 59 (2730 nm)
This work	InF_3	Single-mode	[2700, 5000] nm	50 : 50 (4950 nm)

Future work will explore the performance limits of fluoride fiber couplers with respect to their maximum input power; additionally, the integration of novel 2D materials with fluoride fibers could be also investigated for ultrafast emission [39–42].

5. Conclusion

A single-mode optical fiber coupler has been accurately designed via full vector FEM and supermode theory. The complexity of the waist geometry comprising a capillary and two optical fibers with different degrees of fusion has been taken into account in the simulation. The device has been constructed by means of drawing under controlled heating in a pure environment to mitigate the hygroscopicity of the fluoride glass and ensure low losses. The experimental results show excellent agreement with the simulation, proving, for the first time, a coupling behavior also in the upper wavelength range of transparency of the indium fluoride glass, i.e. $\lambda = 5000$ nm. These results are particularly crucial for different mid-infrared applications, including: (i) in-line fiber lasers; (ii) in-line fiber amplifiers; (iii) ring cavities; (iv) filtering; (v) multiplexing of representative wavelengths in spectroscopy.

Data availability statement

The data that support the findings of this study are available upon reasonable request from the authors.

Acknowledgments

This work was partially supported by ASI 687/2022—MUR 341 15/03/22 'SPACE IT UP' (CUP: D53C24000570006); MIUR PRIN 2022, NRPP—DD n. 1181 del 27-07-2023—InnoVative tEchnoloGies for non-invasivE assessmenT of plAnt healTh conditIon to support precisiOn farmiNg 'VEGETATION' (P2022ZF9P2, CUP: I53D23005710 001); H2020-ICT-37-2020 'Photonic Accurate and Portable Sensor Systems Exploiting Photo-Acoustic and Photo-Thermal Based Spectroscopy for Real-Time Outdoor Air Pollution Monitoring—PASSEPARTOUT' n. 101016956; the European Union under the Italian National Recovery and Resilience Plan (NRRP) of NextGenerationEU, with reference to the partnership on 'Telecommunications of the Future' (PE00000001—program 'RESTART', CUP: D93C22000910001) —STRUCTURAL PROJECT Antennas & Devices foR mixing, dEtection And Manipulation of mmWaves; ASI 2024-68-I.0 'Origami Reconfigurable Beam-steering Antennas with METAsurfaces for Communication on Small Satellites—ORBIT-META' (CUP: F93C24000550001); HORIZON-TMA-MSCA-SE HORIZON

TMA MSCA Staff Exchanges (101182995) 'Cr4+:YAG/Polymer nanocomposite as alternative materials for Q-switched lasers: properties, modeling, and applications—ALTER-Q'.

Conflict of interest

The authors have no conflicts to disclose.

Author contributions

Francesco Anelli 0000-0002-3397-224X
Conceptualization (equal), Data curation (lead), Formal analysis (lead), Methodology (equal), Writing – original draft (lead)

Andrea Annunziato
Conceptualization (equal), Data curation (supporting), Methodology (equal), Writing – review & editing (equal)

Jean Letourneur
Methodology (equal), Writing – review & editing (equal)

Solenn Cozic
Methodology (equal), Writing – review & editing (equal)

Francesco Prudenzano 0000-0001-9347-3218
Conceptualization (equal), Data curation (supporting), Funding acquisition (lead), Methodology (equal), Project administration (lead), Writing – review & editing (equal)

References

[1] Pal B 2003 Fabrication and modeling of fused biconical tapered fiber couplers *Fiber Integr. Opt.* **22** 97–117
[2] Teng J, Yang J, Lv C, Chen T, Guo J, Feng J and Wu P 2014 Guidelines for design and fabrication of fused fiber coupler based wavelength division multiplexings *Opt. Fiber Technol.* **20** 239–44
[3] Chen J-C, Ho C-W and Wang J-S 2016 Optical fiber coupler with a hollow core fiber for magnetic fluid detection *J. Lightwave Technol.* **34** 5220–5
[4] Tsekrekos C P and Syvridis D 2014 Symmetric few-mode fiber couplers as the key component for broadband mode multiplexing *J. Lightwave Technol.* **32** 2461–7
[5] Jager M, Plotner M, Eschrich T, de Vries O, Kobelke J, Schreiber T, Unger S, Eberhardt R, Bartelt H and Tunnermann A 2015 High-brightness incoherent combination of fiber lasers in 7×1 fiber couplers at average powers > 5 kW *J. Lightwave Technol.* **33** 4297–302
[6] Tavakoli F, Rekik A and Rochette M 2017 Broadband and wavelength-dependent chalcogenide optical fiber couplers *IEEE Photonics Technol. Lett.* **29** 735–8
[7] Luo X *et al* 2022 All-fiber mid-infrared supercontinuum generation pumped by ultra-low repetition rate noise-like pulse mode-locked fiber laser *J. Lightwave Technol.* **40** 4855–62
[8] Wang L, Ma W, Zhang P, Zhu L, Yang D, Wang X and Dai S 2019 Mid-infrared gas detection using a chalcogenide suspended-core fiber *J. Lightwave Technol.* **37** 5193–8
[9] Kinjalk K *et al* 2024 Highly selective and sensitive detection of volatile organic compounds using long wavelength InAs-based quantum cascade lasers through quartz-enhanced photoacoustic spectroscopy *Appl. Phys. Rev.* **11** 021427
[10] Zhao Y, Kusama S, Furutani Y, Huang W-H, Luo C-W and Fuji T 2023 High-speed scanless entire bandwidth mid-infrared chemical imaging *Nat. Commun.* **14** 3929
[11] Ishigane G, Toda K, Tamamitsu M, Shimada H, Badarla V R and Ideguchi T 2023 Label-free mid-infrared photothermal live-cell imaging beyond video rate *Light Sci. Appl.* **12** 174
[12] Baker C and Rochette M 2011 A generalized heat-brush approach for precise control of the waist profile in fiber tapers *Opt. Mater. Express* **1** 1065
[13] Stevens G and Woodbridge T 2016 Mid-IR fused fiber couplers *Proc. SPIE* **9730** 973007
[14] Xia C, Xu Z, Islam M N, Terry F L, Freeman M J, Zakel A and Mauricio J 2009 10.5 W time-averaged power mid-IR supercontinuum generation extending beyond 4 μm with direct pulse pattern modulation *IEEE J. Sel. Top. Quantum Electron.* **15** 422–34
[15] Dantanarayana H G, Abdel-Moneim N, Tang Z, Sojka L, Sujecki S, Furniss D, Seddon A B, Kubat I, Bang O and Benson T M 2014 Refractive index dispersion of chalcogenide glasses for ultra-high numerical-aperture fiber for mid-infrared supercontinuum generation *Opt. Mater. Express* **4** 1444
[16] Basaldua I, Kuis R, Burkins P, Jiang Z and Johnson A M 2018 Measurements of the nonlinear refractive index (n2) for indium fluoride (InF3) bulk glass and fiber *Frontiers in Optics/Laser Science* (OSA) p JTu3A.38
[17] Anelli F, Annunziato A, Loconsole A M, Portosi V, Cozic S, du Teilleul P L P, Venck S, Poulain S and Prudenzano F 2024 Low-loss fluoride optical fiber coupler for mid-infrared applications *J. Lightwave Technol.* **42** 2457–63
[18] Rezaei M, Zeweldi G T, Shamim M H M and Rochette M 2023 Single-mode optical fiber couplers made of fluoride glass *Opt. Express* **31** 27183
[19] Séguin A, Becerra-Deana R I, Virally S, Boudoux C and Godbout N 2023 Fabrication and characterization of indium fluoride multimode fused fiber couplers for the mid-infrared *Opt. Express* **31** 33670

[20] Rezaei M, Shamim M H M, Amraoui M E, Messaddeq Y and Rochette M 2022 Nonlinear chalcogenide optical fiber couplers *Opt. Express* **30** 20288
[21] Stepanov B, Benderov O, Tebeneva T, Snopatin G, Spiridonov M and Scripachev I 2018 Chalcogenide optical fiber couplers made by FBT method *J. Non-Cryst. Solids* **480** 23–27
[22] Rezaei M and Rochette M 2019 All-chalcogenide single-mode optical fiber couplers *Opt. Lett.* **44** 5266
[23] Grebnev K, Perminov B, Fernandez T T, Fuerbach A and Chernysheva M 2024 Fluoride and chalcogenide glass fiber components for mid-infrared lasers and amplifiers: breakthroughs, challenges, and future perspective *APL Photonics* **9** 110901
[24] Huang W-P 1994 Coupled-mode theory for optical waveguides: an overview *J. Opt. Soc. Am. A* **11** 963
[25] McIntyre P D and Snyder A W 1973 Power transfer between optical fibers *J. Opt. Soc. Am.* **63** 1518
[26] Xia X, Zhou Y and Madsen C K 2012 Analysis of As2-S3-Ti:LiNbO3 taper couplers using supermode theory *Opt. Photonics J.* **02** 344–51
[27] Lacroix S, Gonthier F and Bures J 1994 Modeling of symmetric 2 × 2 fused-fiber couplers *Appl. Opt.* **33** 8361
[28] Love J D, Henry W M, Stewart W J, Black R J, Lacroix S and Gonthier F 1991 Tapered single-mode fibres and devices. Part 1: adiabaticity criteria *IEE Proc. J. Optoelectron* **138** 343
[29] Ek-Ek J R, Martinez-Pinon F, Alvarez-Chavez J A, Ceballos-Herrera D E, Sanchez-Lara R and Offerhaus H L 2020 Fundamental mode intensity evolution in tapered optical fibres *Laser Phys.* **30** 126204
[30] Chang H, Lin T-H and Wu T-L 1995 Accurate coupling coefficients for fiber couplers with weakly fused cross sections *Appl. Opt.* **34** 6168
[31] Di Bin P and Mothe N 2009 Numerical analysis of directional coupling in dual-core microstructured optical fibers *Opt. Express* **17** 15778
[32] Annunziato A, Anelli F, Teilleul P L P D, Cozic S, Poulain S and Prudenzano F 2022 Fused optical fiber combiner based on indium fluoride glass: perspectives for mid-IR applications *Opt. Express* **30** 44160
[33] Sunder S and Sharma A 2021 Engineering adiabaticity for efficient design of photonic lanterns *IEEE Photonics J.* **13** 1–13
[34] Poulain M 1992 Overview of crystallization in fluoride glasses *J. Non-Cryst. Solids* **140** 1–9
[35] Ducharme É, Virally S, Becerra-Deana R I, Boudoux C and Godbout N 2022 Viscosity of fluoride glass fibers for fused component fabrication *Appl. Opt.* **61** 5031
[36] Anelli F, Annunziato A, Loconsole A M, Venck S, Cozic S and Prudenzano F 2024 Mode-group selective photonic lantern based on indium fluoride optical fibers for mid-infrared *J. Lightwave Technol.* **43** 1–8
[37] Irawan D, Saktioto T, Iwantono M, Juandi M and Ali J 2015 An optimum design of fused silica directional fiber coupler *Optik* **126** 640–4
[38] Annunziato A *et al* 2024 Single-mode fluoroindate coupler for mid-IR applications *Proc. SPIE* **13003** 29
[39] Guo B, Xiao Q, Wang S and Zhang H 2019 2D layered materials: synthesis, nonlinear optical properties, and device applications *Laser Photonics Rev.* **13** 1800327
[40] Li S, Wang C, Yin Y, Lewis E and Wang P 2020 Novel layered 2D materials for ultrafast photonics *Nanophotonics* **9** 1743–86
[41] Wei C, Zhu X, Wang F, Xu Y, Balakrishnan K, Song F, Norwood R A and Peyghambarian N 2013 Graphene Q-switched 278 μm Er^3+-doped fluoride fiber laser *Opt. Lett.* **38** 3233
[42] Wei C, Luo H, Zhang H, Li C, Xie J, Li J and Liu Y 2016 Passively Q-switched mid-infrared fluoride fiber laser around 3μm using a tungsten disulfide (WS_2) saturable absorber *Laser Phys. Lett.* **13** 105108